Sensors and Actuators B 203 (2014) 111–117

Contents lists available at ScienceDirect

Sensors and Actuators B: Chemical

journal homepage: www.elsevier.com/locate/snb

Trimethylamine sensors with enhanced anti-humidity ability fabricated from $La_{0.7}Sr_{0.3}FeO_3$ coated In_2O_3–SnO_2 composite nanofibers

Qi Qi[a], Yong-Cun Zou[a], Mei-Hong Fan[a], Yi-Pu Liu[a], Shuang Gao[a], Pei-Pei Wang[a], Yi He[a], De-Jun Wang[a,b], Guo-Dong Li[a,*]

[a] State Key Lab of Inorganic Synthesis & Preparative Chemistry, College of Chemistry, Jilin University, Changchun 130012, PR China
[b] Department of Chemistry, Tsinghua University, Beijing 100086, PR China

ARTICLE INFO

Article history:
Received 26 February 2014
Received in revised form 19 June 2014
Accepted 20 June 2014
Available online 28 June 2014

Keywords:
Nanofibers
Electrospinning
Semiconductors
Trimethylamine
Gas sensors

ABSTRACT

In_2O_3–SnO_2 composite nanofibers are synthesized via an electrospinning method and coated with $La_{0.7}Sr_{0.3}FeO_3$ nanoparticles. Trimethylamine sensors are fabricated from the coated nanofibers and investigated at various conditions of different humidity. High response and short response/recovery times are obtained at 80 °C. The response is around 8.1 to 1 ppm trimethylamine, and the response and recovery times are about 1 and 6 s, respectively. Especially, the sensors show good humidity-resistant ability. The response only decreases to 6.3 for 1 ppm trimethylamine at 85% RH (25 °C). These characteristics would make the sensors good candidates for trimethylamine detection in practical applications.

1. Introduction

Trimethylamine (TMA, $(CH_3)_3N$) is a colorless, fishlike smell and toxic gas, which is usually produced during the deterioration process of seafood [1–3]. Many research groups have reported that TMA can be used as an effective indicator of seafood quality because its amount increases with the decomposition of trimethyl-N-oxide in seafood after its death [4,5]. Based on the experiential data [6], the fish is fresh when the concentration of TMA is in the range of 0–10 ppm, while it gradually becomes rotten when the concentration of TMA is above 10 ppm. As decayed seafood is related to serious health problems, such as septicemia and gastroenteritis, the detection of TMA is of great importance to food industry. Several techniques (such as pH test, liquid chromatography, ion mobility spectrometry and mass spectrometry) have been employed in the detection of TMA [7–9], but the complex and expensive apparatuses used in these methods are neither portable nor easily assembled, which make them inconvenient for practical application. Accordingly, TMA sensors with tiny structure, low cost, rapid detection and high reliability have received considerable attention in recent years [9].

TMA sensors are usually fabricated from metal oxide semiconductors such as ZnO, TiO_2, Fe_2O_3, SnO_2 and In_2O_3 [7–9]. It is clear that most traditional TMA sensors have two main disadvantages. Firstly, they can only be operated at high temperature (around 300 °C), which is dangerous [8,9]. Because the semiconductors used in these sensors are in the form of nanopowders, they need high energy to activate (Table 1) [8,10–12]. The low responses of these TMA sensors at low temperature have restricted their practical applications. Secondly, the employed semiconductors are also sensitive to H_2O, which is ubiquitous in the environment, thus many TMA sensors can not work at high humidity conditions [9]. This severely limits their applications, especially for portable TMA detection in seafood market.

In this decade, one-dimensional (1D) nanostructures have been proved to be superior candidates compared with powder materials in chemical sensors and biosensors for their high surface energy, effective electron transports and large surface-to-volume ratio [13,14]. In particular, semiconducting nanofibers synthesized by electrospinning have exhibited superior sensitive properties under low temperature [15]. Many low-temperature sensors have been successfully fabricated from electrospun nanofibers, and their response values, response and recovery speeds, selectivity and stability are much better than traditional powder sensors [15–18].

Herein, we report high performance TMA sensors with anti-humidity ability which are assembled from $La_{0.7}Sr_{0.3}FeO_3$ coated

* Corresponding author. Tel.: +86 431 85168318; fax: +86 431 85168624.
E-mail addresses: lgd@jlu.edu.cn, lifind@21cn.com (G.-D. Li).

http://dx.doi.org/10.1016/j.snb.2014.06.082
0925-4005/

Table 1
Comparison of TMA-sensing properties of some topical sensors.

Materials	Operating temperature (°C)	TMA concentration (ppm)	Response	References
ZnO nanoparticles	30	50	6	[10]
WO_3 films	70	50	70	[11]
α-Fe_2O_3/TiO_2	250	50	13.9	[11]
MoO_3 nanoplates	300	5	373.74	[12]
ZnO–In_2O_3 nanofibers	375	5	120	[8]

In_2O_3–SnO_2 composite (LISc) nanofibers. In_2O_3–SnO_2 compounds have been extensively used in solar cells, organic light emitting diodes, photocatalysis, physical and chemical sensors [19–21]. 1D In_2O_3–SnO_2 composite (ISc) nanostructures have been employed in low-temperature detection for ethanol, H_2O and CO [22]. However, the performances of these materials are often affected by humid conditions because both SnO_2 and In_2O_3 are humidity sensing materials [23]. While, $La_{0.7}Sr_{0.3}FeO_3$ nanoparticles, which are highly sensitive to reducing gas, exhibit excellent anti-humidity properties at the same time [24]. By coating $La_{0.7}Sr_{0.3}FeO_3$ on ISc nanofibers, both the TMA sensing performance and anti-humidity ability are enhanced. The corresponding mechanism is further discussed.

2. Experimental

2.1. Synthesis of materials and fabrication of sensors

Sensor substrates were fabricated by radio-frequency (RF) sputtering method, and Pt arrays were formed on SiO_2/Si chips as signal electrodes. The thickness of SiO_2 layer and Pt array were 300 and 100 nm, respectively. The precursor solution was directly electrospun on sensor substrates with interdigitated Pt electrode arrays. The sensor length and width were 3 and 2 mm, respectively.

All chemicals (analytical grade reagents) were purchased from Beijing Chemicals Co. Ltd. and used as received without further purification. Deionized water with a resistivity of 18.0 MΩ cm^{-1} was used in all experiments.

Nanocrystalline $La_{0.7}Sr_{0.3}FeO_3$ was prepared by a citrate method [25]. According to the formula $La_{0.7}Sr_{0.3}FeO_3$, 0.7 mmol of $La(NO_3)_3{\cdot}6H_2O$, 0.3 mmol of $Sr(NO_3)_2$ and 1.0 mmol of $Fe(NO_3)_3{\cdot}9H_2O$ were dissolved in 80 mL of deionized water, and then 15 mg of citric acid was dropped into the mixture. Then, the mixture was heated at 80 °C under stirring for 2 h to obtain a homogeneous precursory sol of $La_{0.7}Sr_{0.3}FeO_3$. ISc nanofibers were prepared by an electrospinning method [26]. Typically, 0.4 g of $In(NO_3)_3{\cdot}4.5H_2O$ and 0.1 g of $SnCl_2{\cdot}2H_2O$ were added to 12.8 g of mixed solvent containing N,N-dimethylformamide (DMF)/ethanol with a weight ratio of 1:1 and stirred for 2 h, and then 1.2 g of PVP was added to the above solution under stirring for another 6 h. Electrospinning of ISc nanofibers was conducted on a similar set-up which was reported in a previous study [27]. The obtained spinning solution was delivered to a hypodermic syringe and modulated to flow at a constant rate of 1.0 mL/h, and then electrospun by applying 20 kV at an electrode distance of 25 cm. A piece of flat aluminum foil was used as the cathode and several sensor substrates were placed on it. After being electrospun for 2 h, the sensor substrates were calcined at 500 °C for 2 h in air and then $La_{0.7}Sr_{0.3}FeO_3$ sol solution was dropped on them at room temperature. Finally, the sensors were calcined at 600 °C for 1 h in air followed by annealing at 300 °C for 10 min in hydrogen atmosphere to obtain the $La_{0.7}Sr_{0.3}FeO_3$-coated ISc nanofiber sensors (LISc nanofiber sensors). Un-coated sensors (ISc nanofiber sensors) and $La_{0.7}Sr_{0.3}FeO_3$ sensors were also fabricated via the same way for comparison.

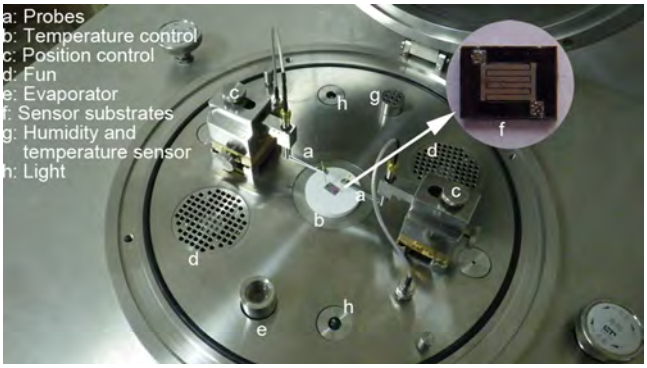

Fig. 1. A photograph of the gas sensing analysis system.

2.2. Characterization of materials and measurement of sensors

X-Ray diffraction (XRD) analysis was conducted on a Rigaku D/Max 2550 X-ray diffractometer with Cu Kα radiation (λ = 1.5418 Å). Scanning electron microscopy (SEM) images were performed on a JEOL JSM 6700F. Transmission electron microscope (TEM) images were obtained on a FEI Tecnai G2S-Twin with a field emission gun operating at 200 kV. N2 adsorption–desorption isotherms were measured at 77 K on a Micromeritics ASAP2020 system. Surface area was evaluated using a Brunauer–Emmett–Teller (BET) method. X-ray photoelectron spectroscopy (XPS) spectra were determined on an ESCALAB 250 X-ray photoelectron spectrometer (Al Kα $h\nu$ = 1486.6 eV). The C 1s at 284.8 eV was used as the reference of standardization.

Sensing measurement was performed on a CGS-1TP (Chemical Gas Sensor-1 Temperature Pressure) intelligent gas sensing analysis system (Beijing Elite Tech Co., Ltd., China) [28]. The analysis system offered an external temperature control, which could adjust the sensor temperature with a precision of 1 °C. Two probes were pressed on sensor electrodes, and the electrical signals were collected through the probes and analyzed by the system automatically. The gas ambience was controlled by a DGD-III (Dynamic Gas Distributing-III) system (Beijing Elite Tech Co., Ltd., China). Dry TMA gas with high purity (99.99%) was the target gas to be tested, and artificially synthesized airs with different relative humidity (RH) levels were employed as the background. The relative humidity values were measured at 25 °C, and the values were also monitored in a real time. A photograph of the sensing measurement is shown in Fig. 1. The sensor response (R) was designated as $R = R_a/R_g$, where R_a and R_g were the sensor resistance in air (base resistance) and a mixture of target gas and air, respectively. The time taken by the sensor resistance to change from R_a to $R_a - 90\% \times (R_a - R_g)$ was defined as response time when the target gas was introduced to the sensor, and the time taken from R_g to $R_g + 90\% \times (R_a - R_g)$ was defined as recovery time when the target gas was replaced by air.

3. Results and discussion

The XRD pattern of LISc nanofibers is shown in Fig. 2. Except the diffraction peaks of SnO_2 and In_2O_3, the diffractions corresponding

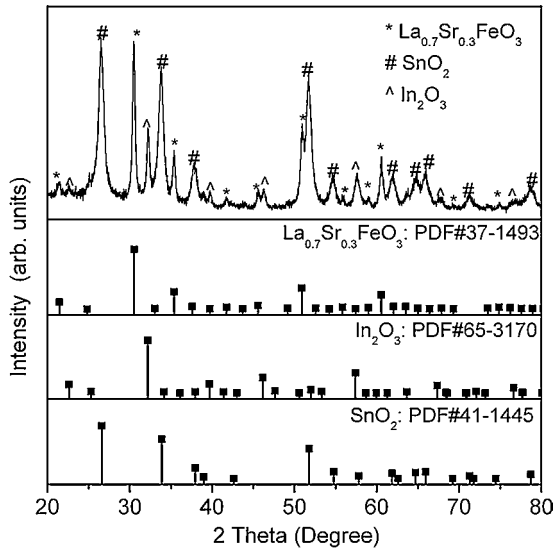

Fig. 2. XRD pattern of LISc nanofibers.

to $La_{0.7}Sr_{0.3}FeO_3$ are also observed. The results suggest that crystalline $La_{0.7}Sr_{0.3}FeO_3$ forms on the surface of ISc nanofibers instead of solid solution, and this may be resulted from different thermal decomposition behaviors between $In(NO_3)_3\,4.5H_2O/SnCl_2$/PVP composite nanofibers and $La(NO_3)_3/Sr(NO_3)_2/Fe(NO_3)_3$/citric acid precursors. Similar phenomena were also found in other reports [29–31]. The phase separation in this process will lead to the formation of heterostructures in the final materials.

$La_{0.7}Sr_{0.3}FeO_3$ nanoparticles show a homogeneous morphology containing nanoparticles with an average size of 20 nm, as shown in Fig. 3(a). SEM and TEM images of ISc nanofibers are given in Fig. 3(b) and (c). The ISc nanofibers with length of several tens of micrometers and diameter ranging from 40 to 100 nm are composed of regular nanoparticles with an average diameter of 25 nm. The nanofibers form a web-like micro-structure naturally with many large pores. After the doping process (Fig. 3(d)), the $La_{0.7}Sr_{0.3}FeO_3$ nanoparticles pack tightly on the surface of ISc nanofibers and therefore more gas-absorbing sites would be formed in the pores [32].

XPS is an effective technique to investigate the surface composition and the chemical state of the elements existing in the products. Fig. 4 (a) shows the In 3d spectrum at 444.6 eV (In $3d_{5/2}$) and 452.1 (In $3d_{3/2}$). Fig. 4(b) shows the high resolution spectrum of Sn 3d at 495.5 eV (Sn $3d_{3/2}$) and 487.1 eV (Sn $3d_{5/2}$). High resolution spectrum of La $3d_{5/2}$ has two binding energy peaks located at 834.7 eV and 837.9 eV, and the two peaks of La $3d_{3/2}$ are located at 851.4 eV and 854.5 eV (Fig. 4(c)). The lower ones in the doublet of La 3d (5/2) and La 3d (3/2) can be assigned to shake-up satellite, which results from the 2p electrons of oxygen transfer to the empty 4f orbit of lanthanum [33,34]. The peak located at 719.5 eV is the characteristic peak of Fe 2p for Fe^{3+}, as shown in Fig. 4(d).

Sensor responses were examined as a function of operating temperature to determine the optimum working condition. The testing chamber was controlled at 30% RH (25 °C). As shown in Fig. 5, $La_{0.7}Sr_{0.3}FeO_3$ sensors do not response to TMA in the tests because $La_{0.7}Sr_{0.3}FeO_3$ is quite chemical-stable below 100 °C [24]. ISc nanofiber sensors show the highest response of 4 to 1 ppm TMA at room temperature (25 °C). ISc nanofibers are room-temperature sensing materials, and high temperature will change their surface oxygen species thus decrease its sensing response accordingly [22]. To LISc nanofiber sensors, the response increases with the increase of operating temperature and attains a maximum at 80 °C, followed by a decrease with a further increase of operating

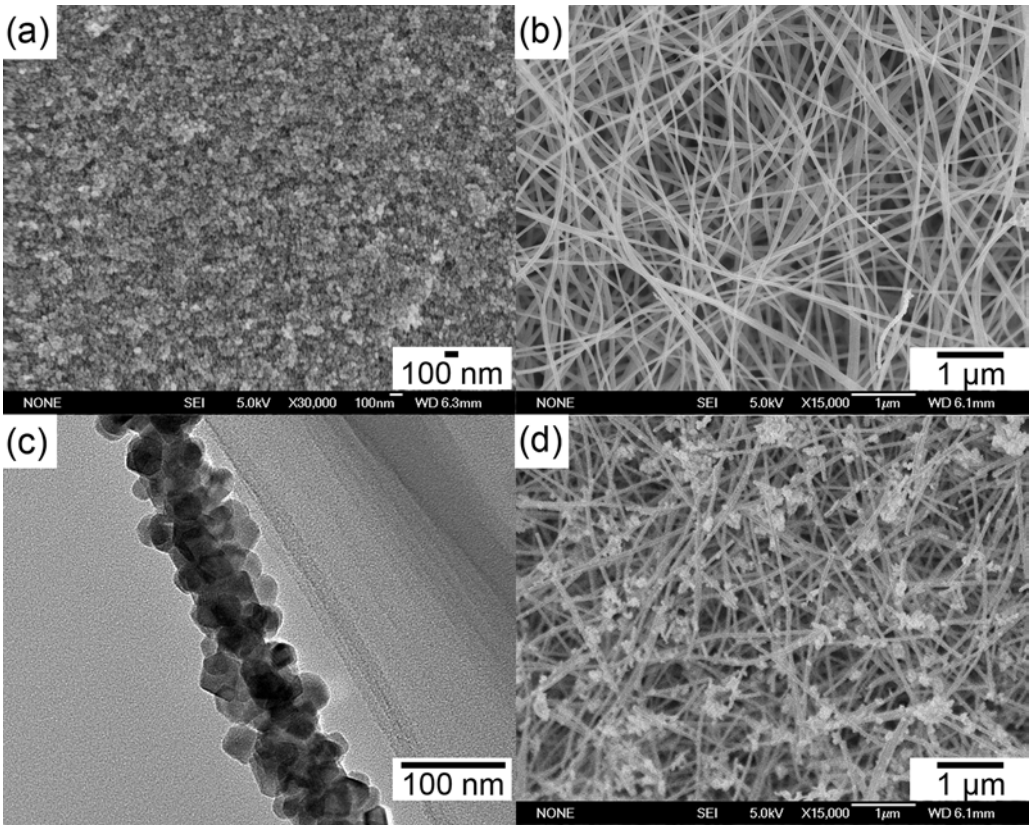

Fig. 3. SEM images of $La_{0.7}Sr_{0.3}FeO_3$ nanoparticles (a), ISc nanofibers (b), and LISc nanofibers (d). A TEM image of ISc nanofibers (c).

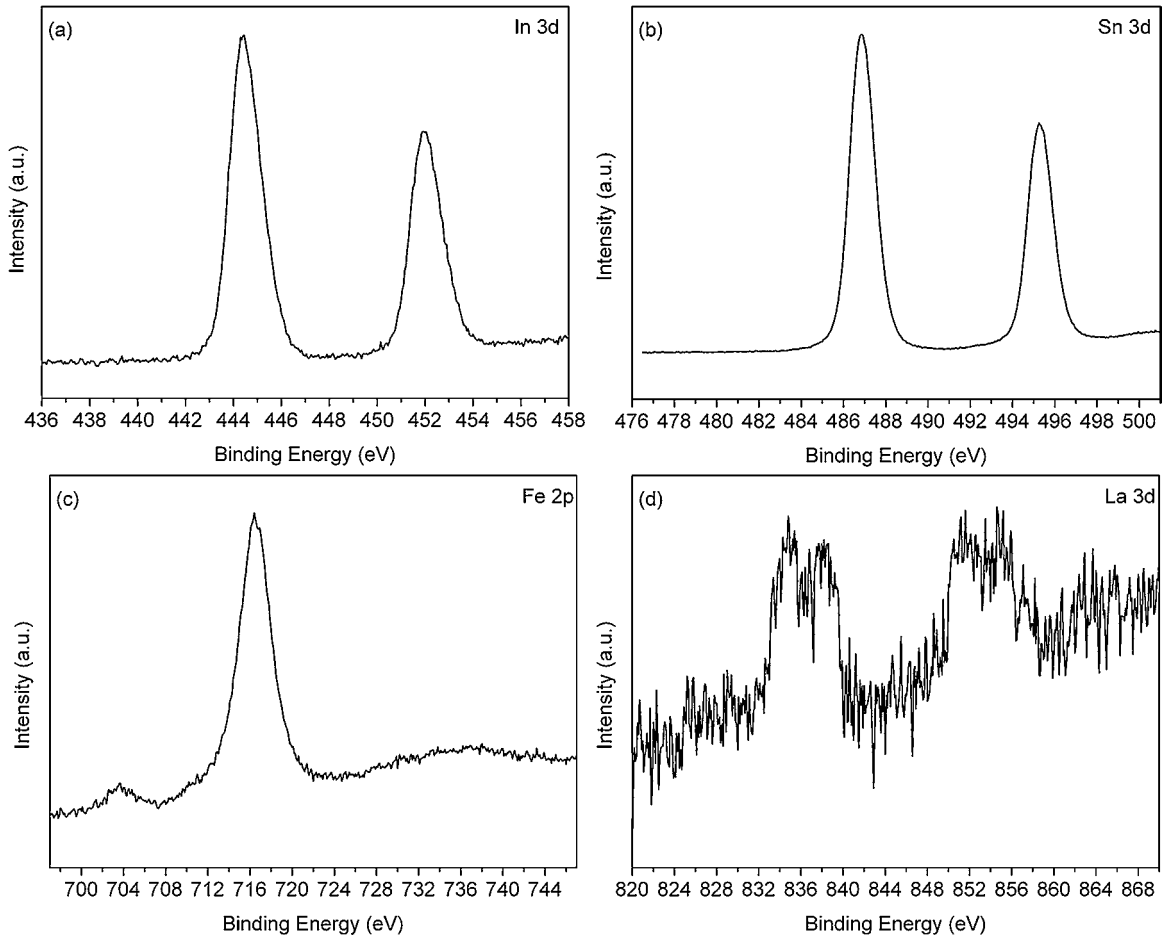

Fig. 4. XPS spectra of (a) In 3d, (b) Sn 3d, (c) Fe 2p, and (d) La 3d for LISc nanofibers.

temperature. Therefore, the optimum operating temperatures of ISc nanofiber sensors and LISc nanofiber sensors are determined to be 25 and 80 °C, respectively. ISc is a kind of low-temperature-working material, and the corresponding nanofibers or thin films show high responses to many gases (such as ethanol, NH_3, NO_2 and H_2) at room temperature [19]. This is mainly caused by the higher surface activation energy of ISc than that of binary oxides [21]. Coating $La_{0.7}Sr_{0.3}FeO_3$ nanoparticles on ISc nanofibers not only provides more adsorbing sites on smooth ISc nanofibers (as shown in Fig. 3(d)), but also forms heterojunctions and increases the chemical reactivity or preference chemical absorbing ability accordingly. Besides, preference chemisorption of TMA on $La_{0.7}Sr_{0.3}FeO_3$ by donating electrons to $La_{0.7}Sr_{0.3}FeO_3$ is also a possible mechanism.

Fig. 6 shows transient response curves of the LISc nanofiber sensors upon the introduction and removal of 50 ppb, 1 ppm and 2 ppm TMA at 80 °C (30% RH, 25 °C). The sensors show the n-type sensing behavior and reversible sensing performance. The responses are about 1.3, 8.1 and 10.2 to 50 ppb, 1 ppm and 2 ppm TMA. And the sensor resistance can go back to the initial value in the continuous

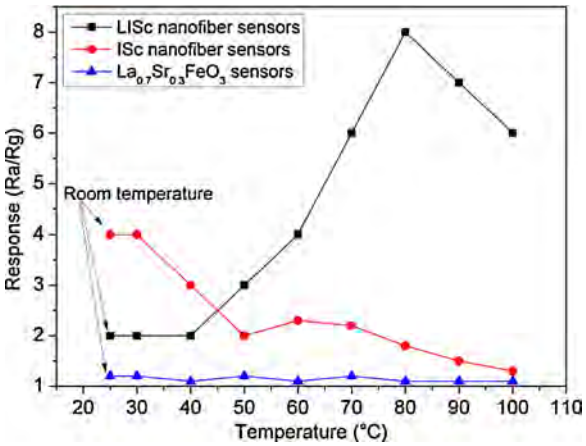

Fig. 5. Responses of LISc nanofiber sensors, ISc nanofiber sensors, $La_{0.7}Sr_{0.3}FeO_3$ sensors to 1 ppm TMA at different temperatures.

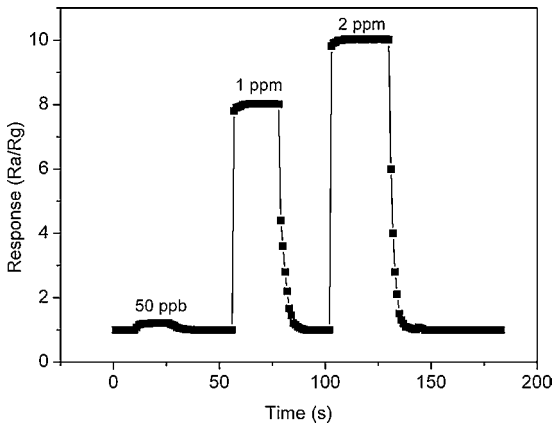

Fig. 6. Response–time curves of LISc nanofiber sensors to 50 ppb, 1 ppm and 2 ppm TMA at 80 °C.

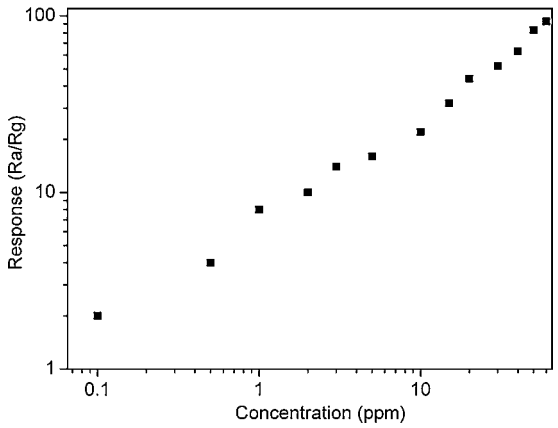

Fig. 7. Responses of LISc nanofiber sensors to different concentrations of TMA at 80 °C.

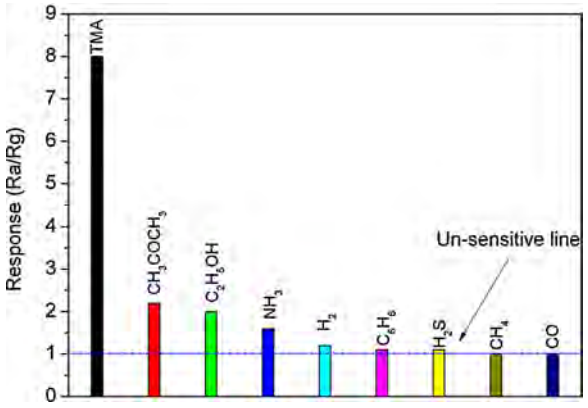

Fig. 8. Responses of LISc nanofiber sensors to 1 ppm different gases at 80 °C.

tests. The response time is less than 1 s, and the recovery time is about 8 s. Such a rapid response at a relatively low temperature mainly benefits from the 1D nanostructure of the ISc nanofibers [13]. The high penetrability and oriented signal-transmission make the response time much shorter than many other ISc nanofiber sensors. And $La_{0.7}Sr_{0.3}FeO_3$ nanoparticles on the fiber surface can also improve the absorption and activation properties of the ISc nanofibers. Those advantages lead to a significant improvement of the fast response of the as-prepared sensors.

LISc nanofiber sensors exhibit extremely high responses to TMA at 30% RH (25 °C), as shown in Fig. 7. For instance, the responses are 1.2, 2, 8, and 22 to 50 ppb, 100 ppb, 1 ppm, and 10 ppm TMA, respectively. These values are much higher than those of other sensing materials reported previously. Especially, the sensors show a linear response-TMA concentration calibration curve in the range of 50 ppb–60 ppm. In fact, the response of semiconducting oxide gas sensitive sensors can usually be empirically represented as $R = A[C]^N + B$, where A and B are constants and $[C]$ is the concentration of the target gas. N usually has a value in the range of 0.5–1.0, depending on the charge species of the surface and the stoichiometry of the elementary reactions on the surface [27]. For the current sensors, N is around 0.72 for TMA below 60 ppm, suggesting that the LISc nanofiber sensors are suitable for detecting TMA of low concentrations.

The responses to 1 ppm different gases are also measured for LISc nanofiber sensors at 80 °C, as shown in Fig. 8. The sensors exhibit excellent selectivity to these common interference gases at 30% RH (25 °C). The corresponding responses of the sensors to TMA, CH_3COCH_3, C_2H_5OH, NH_3, H_2, C_6H_6, H_2S, CH_4 and CO are 8.1, 2.2, 2, 1.6, 1.2, 1.1, 1.1, 1.0 and 1.0, respectively. This high selectivity may be resulted from the changed optimized working temperature and the heterojunctions brought by $La_{0.7}Sr_{0.3}FeO_3$ coating [8].

TMA sensors are mainly used to test the quality of seafood, thus various environments are involved in practice such as supermarket, storeroom and springhouse, which usually have a high humidity. Accordingly, the anti-humidity property of TMA sensors is vital. As shown in Fig. 9, the ISc nanofiber sensors own a response of 4.2 to 1 ppm TMA at 30% RH, but are insensitive at 85% high RH. This is because both In_2O_3 and SnO_2 are humidity sensing materials, and their working temperature is only 25 °C. Contrastively, the LISc nanofiber sensors exhibit much better sensing properties at high humidity. The responses only decrease from 8.1 to 6.3 at 85% RH. The improved anti-humidity properties are related to the higher working temperature of LISc nanofiber sensors. The concentration of water molecules around the sensors will decrease under higher working temperatures due to the change of saturated vapor pressure [21]. And $La_{0.7}Sr_{0.3}FeO_3$ is a highly anti-humidity material which has excellent sensing properties even at 95% RH [22].

The sensing measurements were repeated every 10 days for 60 days to learn the stability of LISc nanofiber sensors. The sensors show nearly constant responses to the target gases at 30% RH (25 °C) in the tests (Fig. 10), confirming their excellent stabilities.

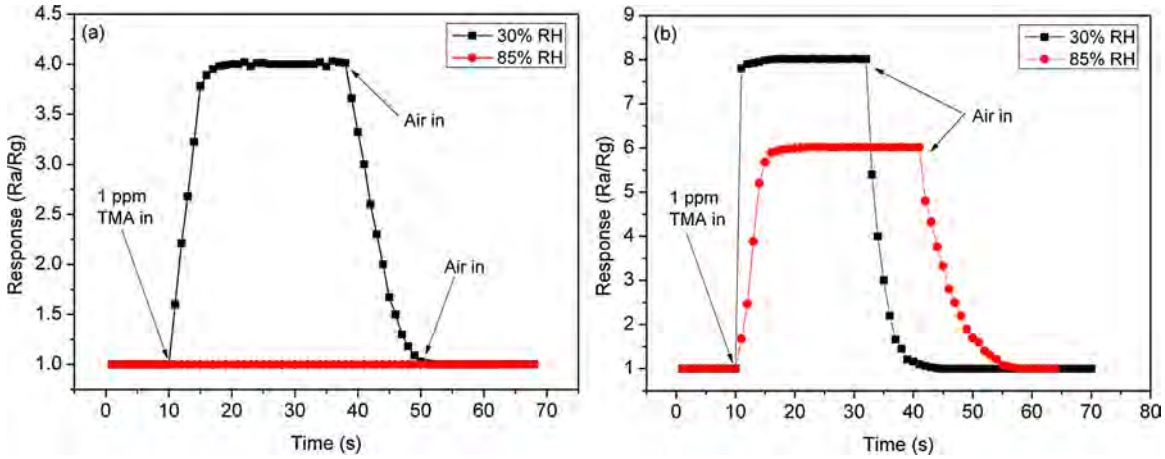

Fig. 9. Response–time curves of ISc nanofiber sensors (operating at 25 °C) to 1 ppm TMA at 30% and 85% RH (a), and response–time curves of LISc nanofiber sensors (operating at 80 °C) to 1 ppm TMA at 30% and 85% RH (b).

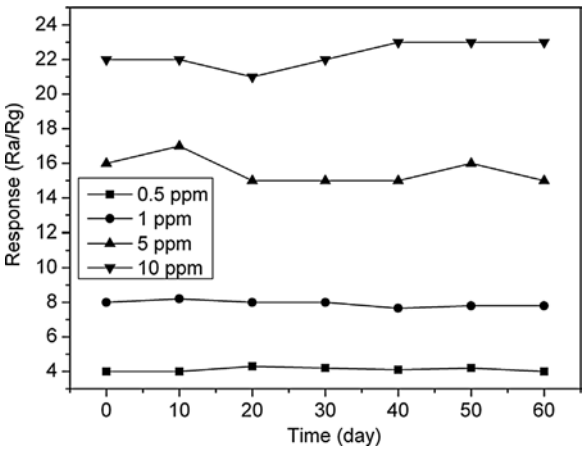

Fig. 10. Stability of LISc nanofiber sensors at 80 °C in 60 days.

In the past six decades, metal oxides have been widely selected for the gas sensing applications. Their sensing mechanism is related to the oxygen adsorption/on the sensor surface [35]. In this case, both In_2O_3 and SnO_2 are typical gas sensing materials. Oxygen molecules, which are chemisorbed on ISc nanofibers, can generate oxygen species and make the nanofibers less conductive. When the nanofibers are exposed to TMA, TMA molecules may react with the chemisorbed oxygen species and release the trapped electron back to the conduction band. Accordingly, the decreased resistances of the sensors are observed [35,36]. This trend was mainly attributed to the reducing nature of TMA and increasing the charge carrier concentration as, represented by the following reaction mechanism:

$$4(CH_3)_3N + 21O_2(surf)^- \rightarrow 2N_2 + 12CO_2 + 18H_2O + 21e^- \quad (1)$$

The addition of SnO_2 into In_2O_3 has been known to be effective in modifying their electrical properties. In_2O_3–SnO_2 system often shows low-working temperatures and high responses in many chemical sensors due to the high catalytic activities coupled with the enhanced vacant oxygen rates [37]. However, the unsolved problems such as low-selectivity and humidity-interference limit their practical applications and also puzzle many researchers [38]. $La_{0.7}Sr_{0.3}FeO_3$ nanoparticles have excellent anti-humidity properties and many commercial gas sensors are fabricated from this type of material [38]. Coating $La_{0.7}Sr_{0.3}FeO_3$ nanoparticles on ISc nanofibers can not only decrease the humidity-interference on the sensors, but also raise the optimized-operating-temperature and improve their selectivity accordingly [39]. Thus, the high performance of the as-fabricated sensors can be attributed to the co-effect of the In_2O_3–SnO_2 systems and the $La_{0.7}Sr_{0.3}FeO_3$ coating treatment.

4. Conclusions

ISc nanofibers are synthesized via an electrospinning method. Coating $La_{0.7}Sr_{0.3}FeO_3$ nanoparticles on ISc nanofibers can effectively improve their TMA sensing properties. Sensors with optimized-operating-temperature, higher response and better anti-humidity have been obtained. The response is 8.1 to 1 ppm TMA and the response and recovery times are only 1 and 6 s, respectively. The response only decreases to 6.3 for 1 ppm TMA at 85% RH (25 °C). The results show a possible route to improve the gas sensing properties of In_2O_3–SnO_2 sensors.

Acknowledgements

This work is supported by the National Natural Science Foundation of China (21371070), the National Basic Research Program of China (973 Program) (2013CB632403) and Jilin Province Science and Technology Development Projects (20140101041JC, 20130204001GX).

References

[1] Y. Takao, M. Nakanishi, T. Kawaguchi, Y. Shimizu, M. Egashira, Semiconductor dimethylamine gas sensors with high sensitivity and selectivity, Sens. Actuators B Chem. 24–25 (1995) 375–379.
[2] K.L.A. Kumar, S. Durgajanani, B.G. Jeyaprakash, J.B.B. Rayappan, Nanostructured ceria thin film for ethanol and trimethylamine sensing, Sens. Actuators B Chem. 177 (2013) 19–26.
[3] K.L. Choi, H.R. Kim, J.H. Lee, Enhanced CO sensing characteristics of hierarchical and hollow In_2O_3 microspheres, Sens. Actuators B Chem. 138 (2009) 497–503.
[4] C.W. Na, S.Y. Park, J.H. Lee, Punched ZnO nanobelt networks for highly sensitive gas sensors, Sens. Actuators B Chem. 174 (2012) 495–499.
[5] R.S. Niranjan, M.S. Londhe, A.B. Mandale, S.R. Sainkar, L.S. Prabhumirashi, K. Vijayamohannan, I.S. Mulla, Trimethylamine sensing properties of thorium-incorporated tin oxide, Sens. Actuators B Chem. 87 (2002) 406–413.
[6] R. Yang, X. Huang, Z.Y. Wang, Y.Z. Zhou, L.T. Liu, A chemisorption-based microcantilever chemical sensor for the detection of trimethylamine, Sens. Actuators B Chem. 145 (2010) 474–479.
[7] X.F. Chu, S.M. Liang, W.Q. Sun, W.B. Zhang, T.Y. Chen, Q.F. Zhang, Trimethylamine sensing properties of sensors based on MoO_3 microrods, Sens. Actuators B Chem. 148 (2010) 399–403.
[8] Y.H. Cho, Y.C. Kang, J.H. Lee, Highly selective and sensitive detection of trimethylamine using WO_3 hollow spheres prepared by ultrasonic spray pyrolysis, Sens. Actuators B Chem. 176 (2013) 971–977.
[9] S.Y. Zhao, P.H. Wei, S.H. Chen, Enhancement of trimethylamine sensitivity of MOCVD-SnO_2 thin film gas sensor by thorium, Sens. Actuators B Chem. 62 (2000) 117–120.
[10] K. Subbulakshmi, R. Pandeeswari, B.G. Jeyaprakash, Surface morphology dependent TMA sensing response of spray deposited ZnO thin films, Superlattices Microstruct. 65 (2014) 219–226.
[11] Z. Lou, F. Li, J. Deng, L.L. Wang, T. Zhang, Branch-like hierarchical heterostructure (α-Fe_2O_3/TiO_2): a novel sensing material for trimethylamine gas sensors, ACS Appl. Mater. Interfaces 5 (2013) 12310–12316.
[12] Y.H. Cho, Y.N. Ko, Y.C. Kang, I.D. Kim, J.H. Lee, Ultraselective and ultrasensitive detection of trimethylamine using MoO_3 nanoplates prepared by ultrasonic spray pyrolysis, Sens. Actuators B Chem. 195 (2014) 189–196.
[13] X.J. Huang, Y.K. Choi, Chemical sensors based on nanostructured materials, Sens. Actuators B Chem. 122 (2007) 659–671.
[14] X. Lu, C. Wang, Y. Wei, One-dimensional composite nanomaterials: synthesis by electrospinning and their applications, Small 5 (2009) 2349–2370.
[15] B.Y. Wei, M.C. Hsu, P.G. Su, H.M. Lin, R.J. Wu, H.J. Lai, A novel SnO_2 gas sensor doped with carbon nanotubes operating at room temperature, Sens. Actuators B Chem. 101 (2004) 81–89.
[16] A. Kolmakov, M. Moskovits, Chemical sensing and catalysis by one-dimensional metal-oxide nanostructures, Annu. Rev. Mater. Res. 34 (2004) 151–180.
[17] H.A. Khorami, M. Keyanpour-Rad, M.R. Vaezi, Synthesis of SnO_2/ZnO composite nanofibers by electrospinning method and study of its ethanol sensing properties, Appl. Surf. Sci. 257 (2011) 7988–7992.
[18] S. Wang, Y. Xiao, D. Shi, H.K. Liu, S.X. Dou, Fast response detection of H_2S by CuO-doped SnO_2 films prepared by electrodeposition and oxidization at low temperature, Mater. Chem. Phys. 130 (2011) 1325–1328.
[19] J. Zhang, J.Q. Hu, F.R. Zhu, H. Gong, S.J. O'Shea, ITO thin films coated quartz crystal microbalance as gas sensor for NO detection, Sens. Actuators B Chem. 87 (2002) 159–167.
[20] N.G. Patel, P.D. Patel, V.S. Vaishnav, Indium tin oxide (ITO) thin film gas sensor for detection of methanol at room temperature, Sens. Actuators B Chem. 96 (2003) 180–189.
[21] S.K. Mishra, D. Kumari, B.D. Gupta, Surface plasmon resonance based fiber optic ammonia gas sensor using ITO and polyaniline, Sens. Actuators B Chem. 171-172 (2012) 976–983.
[22] S. Xu, Y. Shi, Low temperature high sensor response nano gas sensor using ITO nanofibers, Sens. Actuators B Chem. 143 (2009) 71–75.
[23] S.M. Lee, Y.S. Lee, C.H. Shim, N.J. Choi, B.S. Joo, K.D. Song, J.S. Huh, D.D. Lee, Three electrodes gas sensor based on ITO thin film, Sens. Actuators B Chem. 93 (2003) 31–35.
[24] D.V. Karpinsky, I.O. Troyanchuk, K. Bärner, H. Szymczak, M. Tovar, Crystal structure and magnetic ordering of the $LaCo_{1-x}Fe_xO_3$ system, J. Phys. Condens. Matter 17 (2005) 7219–7226.
[25] S. Royer, A. Van Neste, R. Davidson, S. McIntyre, S. Kaliaguine, Methane oxidation over nanocrystalline $LaCo_{1-x}Fe_xO_3$: resistance to SO_2 poisoning, Ind. Eng. Chem. Res. 43 (2004) 5670–5680.
[26] D. Li, Y. Xia, Electrospinning of nanofibers: reinventing the wheel? Adv. Mater. 16 (2004) 1151–1170.

[27] Q. Qi, Y. Feng, T. Zhang, X. Zheng, G. Lu, Influence of crystallographic structure on the humidity sensing properties of KCl-doped TiO_2 nanofibers, Sens. Actuators B Chem. 139 (2009) 611–617.
[28] X.J. Zhang, G.J. Qiao, High performance ethanol sensing films fabricated from ZnO and In_2O_3 nanofibers with a double-layer structure, Sens. Actuators B Chem. 258 (2012) 6643–6647.
[29] B. Ding, M. Wang, X. Wang, J. Yu, G. Sun, Electrospun nanomaterials for ultrasensitive sensors, Mater. Today 13 (2010) 16–27.
[30] K.W. Kim, P.S. Cho, S.J. Kim, J.H. Lee, C.Y. Kang, J.S. Kim, S.J. Yoon, The selective detection of C_2H_5OH using SnO_2–ZnO thin film gas sensors prepared by combinatorial solution deposition, Sens. Actuators B Chem. 123 (2007) 318–324.
[31] Q. Qi, J. Zhao, R.F. Xuan, P.P. Wang, L.L. Feng, L.J. Zhou, D.J. Wang, G.D. Li, Sensitive ethanol sensors fabricated from p-type $La_{0.7}Sr_{0.3}FeO_3$ nanoparticles and n-type SnO_2 nanofibers, Sens. Actuators B Chem. 191 (2014) 659–665.
[32] M.E. Franke, T.J. Koplin, U. Simon, Metal and metal oxide nanoparticles in chemiresistors: does the nanoscale matter? Small 2 (2006) 36–50.
[33] P.J. Yao, J. Wang, H.Y. Du, J.Q. Qi, Synthesis, characterization and formaldehyde gas sensitivity of $La_{0.7}Sr_{0.3}FeO_3$ nanoparticles assembled nanowires, Mater. Chem. Phys. 134 (2012) 61–67.
[34] D.V. Lvanov, L.G. Pinaeva, L.A. Lsupova, E.M. Sadovskaya, I.P. Prosvirin, E.Yu. Gerasimov, I.S. Yakovleva, Effect of surface decoration with $LaSrFeO_4$ on oxygen mobility and catalytic activity of $La_{0.4}Sr_{0.6}FeO_{3-\delta}$ in high-temperature N_2O decomposition, methane combustion and ammonia oxidation, Appl. Catal. A Gen. 457 (2013) 42–51.
[35] H. Liu, S. Wu, S. Gong, J. Zhao, J. Liu, D. Zhou, Nanocrystalline In_2O_3–SnO_2 thick films for low-temperature hydrogen sulfide detection, Ceram. Int. 37 (2011) 1889–1894.
[36] Z. Jiao, M. Wu, J. Gu, X. Sun, The gas sensing characteristics of ITO thin film prepared by sol–gel method, Sens. Actuators B Chem. 94 (2003) 216–221.
[37] B.C. Kim, J.Y. Kim, D.D. Lee, J.O. Lim, J.S. Huh, Effects of crystal structures on gas sensing properties of nanocrystalline ITO thick films, Sens. Actuators B Chem. 89 (2003) 180–186.
[38] C.W. Lin, H.I. Chen, T.Y. Chen, C.C. Huang, C.S. Hsu, R.C. Liu, W.C. Liu, On an indium-tin-oxide thin film based ammonia gas sensor, Sens. Actuators B Chem. 160 (2011) 1481–1484.
[39] Y. Zheng, J. Wang, P. Yao, Formaldehyde sensing properties of electrospun NiO-doped SnO_2 nanofibers, Sens. Actuators B Chem. 156 (2011) 723–730.

Biographies

Qi Qi received his Ph.D. degree in the field of microelectronics and solid state electronics in 2010 from Jilin University. Now, he is carrying out a postdoctoral research related to the synthesis of 1D sensing materials in college of chemistry, Jilin University.

Yong-Cun Zou received his M.S. degree from North East Normal University in 2009. He entered the Ph.D. course in September 2010, Jilin University. He is majored in the preparation of porous materials.

Mei-Hong Fan received her B.S. degree from department of chemistry, Anyang Normal University in 2013. Now, she is a postgraduate student in college of chemistry, Jilin University. She is majored in the synthesis of nanomaterials.

Yi-Pu Liu is an undergraduate student at College of Chemistry, Jilin University in China. Her research interest is the synthesis of advanced functional materials.

Shuang Gao received her B.S. degree from department of chemistry, Harbin Normal University in 2013. Now, she is a postgraduate student in college of chemistry, Jilin University. She is majored in the preparation of composite materials.

Pei-Pei Wang received her B.S. degree from the college of chemistry, Northeast Dianli University, China in 2010. She entered the Ph.D. course in September 2012, Jilin University. She is majored in the synthesis of sensing nanocomposites.

Yi He is a full professor at College of Chemistry, Jilin University in China. She received her B.Sc. (1989), M.Sc. (1994) from Northeast Normal University and Ph.D. (2006) from Jilin University. Her interests include chemical sensor and related materials.

De-Jun Wang is a full professor of physical chemistry at College of Chemistry, Jilin University in China. He received his B.Sc. (1977), M.Sc. (1983) and Ph.D. (1989) from Jilin University. His interests include photoelectric sensors, photocatalysts and related materials.

Guo-Dong Li received his Ph.D. degree in the field of Chemistry in 2001 from Jilin University. He was appointed a full professor in College of Chemistry, Jilin University in 2006. Now, he is interested in the field of sensing functional materials and chemical sensors.